










# Development of bozepinib-loaded nanocapsules for nose-to-brain delivery: preclinical evaluation in glioblastoma

Amanda de Fraga Dias<sup>1</sup> , Danieli Rosane Dallemole<sup>2</sup> , Franciele Aline Bruinsmann<sup>2</sup> , Luiz Fernando Lopes Silva<sup>1</sup> , Olga Cruz-López<sup>3,4</sup> , Ana Conejo-García<sup>3,4</sup> , Ana Maria Oliveira Battastini<sup>1</sup> , Joaquín María Campos<sup>3,4</sup> , Silvia Stanisçuaski Guterres<sup>2</sup> , Adriana Raffin Pohlmann<sup>2</sup>  & Fabrício Figueiró<sup>\*,1,5</sup> 

<sup>1</sup>Programa de Pós-Graduação em Ciências Biológicas: Bioquímica, Instituto de Ciências Básicas da Saúde, Universidade Federal do Rio Grande do Sul, Porto Alegre, RS, Brazil

<sup>2</sup>Programa de Pós-Graduação em Ciências Farmacêuticas, Faculdade de Farmácia, Universidade Federal do Rio Grande do Sul, Porto Alegre, RS, Brazil

<sup>3</sup>Departamento de Química Farmacéutica y Orgánica, Facultad de Farmacia, c/Campus de Cartuja s/n, Granada, Spain

<sup>4</sup>Instituto de Investigación Biosanitaria de Granada (ibs.GRANADA), Granada, Spain

<sup>5</sup>Departamento de Bioquímica, Instituto de Ciências Básicas da Saúde, Universidade Federal do Rio Grande do Sul, Porto Alegre, RS, Brazil

\*Author for correspondence: Tel.: +55 513 308 5554; [fabricao.figueiro@ufrgs.br](mailto:fabricao.figueiro@ufrgs.br)

**Aim:** To develop and characterize bozepinib-loaded lipid-core nanocapsules (BZP-LNC<sup>+</sup>) as a potential treatment for glioblastoma (GBM). **Methods:** Characterization of nanocapsules was performed by diameter, polydispersity index, zeta potential, pH and encapsulation efficiency. GBM cell viability, cell cycle and Annexin/PI were evaluated after BZP-LNC<sup>+</sup> treatment. Synergism between BZP-LNC<sup>+</sup> and temozolomide (TMZ) was performed by CompuSyn software and confirmed *in vitro* and *in vivo*. **Results:** BZP-LNC<sup>+</sup> showed adequate particle sizes, positive zeta potential, narrow size distribution and high encapsulation efficiency. BZP-LNC<sup>+</sup> reduces GBM growth by inducing apoptosis. BZP-LNC<sup>+</sup> and TMZ showed synergistic effect *in vitro* and reduced the *in vivo* glioma growth by approximately 81%. **Conclusion:** The present study provides proof-of-principle insights for the combination of these drugs for GBM treatment.

First draft submitted: 27 April 2021; Accepted for publication: 16 July 2021; Published online: 15 September 2021

**Keywords:** bozepinib • drug delivery • glioblastoma • intranasal • lipid-core nanocapsules • temozolomide

Glioblastoma (GBM) is the most prevalent, malignant and highly aggressive primary brain tumor that affects adults [1]. The standard-of-care therapy includes surgical resection followed by radiotherapy and chemotherapy with temozolomide (TMZ) [2,3]. TMZ is a small and lipophilic second-generation oral alkylating agent that is able to readily cross the blood–brain barrier (BBB) and achieve brain and cerebral spinal fluid levels up to 40% of plasma concentrations. It is the standard first-line chemotherapy for the clinical treatment of GBM since the US FDA approved its efficacy in 2005 [2]. However, GBM treatment is limited by its high heterogeneity, fast proliferation and infiltrating capacity, as well as chemoresistance, leading to inevitable tumor recurrence [4,5]. For this reason, the median overall survival of GBM patients after the treatment is still very low, between 12.1 and 14.6 months after the initial diagnosis, and despite the efforts that have been made in recent decades to prolong the overall survival of patients affected by GBM, this tumor remains currently incurable [6–8]. Therefore, finding new pharmacological approaches are an urgent global health need.

Bozepinib (BZP) is a highly potent and selective anticancer compound made up of a benzo-fused seven-membered ring and the purine moiety [(*RS*)-2,6-dichloro-9-[1-(*p*-nitrobenzene sulfonyl)-1,2,3,5-tetrahydro-4,1-benzoxazepin-3-yl]-9*H*-purine] [9]. Recent findings have shown that BZP induces cell death by apoptosis in breast and colon cancer cells through the activation of a double-stranded RNA-dependent protein kinase (PKR) and

inhibitory effect over kinases involved in carcinogenesis, proliferation and angiogenesis – more specifically by HER2, JNK and ERKs kinase inhibition [9–11]. In addition, it has an inhibitory effect on Akt and VEGF together with antiangiogenic and antimigratory activities [10,11]. Interestingly, BZP is able to abrogate cancer stem cells (CSC) expressing aldehyde dehydrogenases in the low micromolar range in breast and colon cancer cells [10,11]. Lastly, BZP shows *in vivo* antitumor and antimetastatic activity in xenotransplanted nude mice without presenting systemic toxicity [10,11]. This study group has recently shown that BZP has cytotoxic activity in GBM cells (C6 and U138 cell lines) with low IC<sub>50</sub> values compared with nontumor cells. BZP treatment induces apoptosis caspase-dependent, NF-κB pathway activation and a positive CSCs marker, CD133. Interestingly, after two cycles of treatment, BZP was able to eliminate resistant cells expressing NF-κB and CD133<sup>+</sup> [12].

However, according to the Molinspiration server (<http://www.molinspiration.com>) BZP possesses some chemical properties that would limit BBB permeation, such as lipophilicity, which is correlated with the ability of drugs to cross the BBB; it is usually optimal if the Log p-values are in the range of 1.5–2.7 [13,14]; BZP presents log p of 4.03. In addition, with regard to molecular weight (Mw), small molecules may undergo significant passive lipid-mediated transport through the BBB when the Mw is  $\leq 450$  g/mol<sup>-1</sup> [13–15], and BZP has an Mw of 521.33 g/mol<sup>-1</sup>. Another issue is that hydrogen bonding properties can significantly influence the absorption profile of a compound in the CNS, with the ideal number of hydrogen bond donors (nOHNH) being <3 and the number of hydrogen bond acceptors (nON) being <7 [14–16]. BZP presents nOHNH = 0 and nON = 11. Finally, molecular topological polar surface area (TPSA) has been used as a predictor for BBB penetration by many investigators [14,17,18]. In general, drugs aimed at the CNS tend to have a polar surface area estimated at 60–70 Å<sup>2</sup>; BZP presents TPSA of 136.05 Å<sup>2</sup>. In this context, the incorporation of BZP into nanocapsules arises as an alternative for overcoming physicochemical limitations, increasing their bioavailability and antiglioma activity.

Nanotechnology has received intense attention in recent years and has been proposed as an effective strategy for improving drug solubility, effectively targeting cancer cells and overcoming physiological barriers, with more potent and less toxic results [19–21]. Among various nanoparticles (NP), lipid-core nanocapsules (LNC) are a specific kind of nontoxic nanocapsule, formed by a core-shell structure whose core is an organogel (sorbitan monostearate dispersed in capric/caprylic triglyceride), surrounded by a poly(ε-caprolactone) wall, and stabilized by polysorbate 80 micelles at the particle/water interface [22–24]. Additionally, to enhance stability, as well as their biological properties, the external surface of the LNCs can be modified with molecules endowed with specific characteristics, such as chitosan. Chitosan is a polysaccharide of natural origin, obtained from the partial deacetylation of chitin, which is produced from crustacean exoskeletons or fungal cell walls [25,26]. Chitosan is considered a biocompatible, nontoxic and nonallergenic material with adhesive and absorptive properties for mucous membranes [27,28]. The use of chitosan-coated LNCs for intranasal administration has been intensely investigated for the treatment of CNS diseases and has demonstrated significant advantages compared with conventional routes of drug administration [29,30]. Intranasal administration is a promising strategy for circumventing the presence of the BBB – which is impermeable for most molecules – by delivering the drugs directly to the brain along the olfactory and trigeminal nerves, which are in direct contact with the CNS through the olfactory bulb and brainstem, respectively [30–32]. In addition, nasal drug delivery has other advantages, such as ease of administration, noninvasiveness, good patient acceptability, rapid onset of action, relatively large and permeable absorption surface and reduced hepatic first-pass metabolism [32].

In this context, the aim of this study has been to develop and characterize chitosan-coated lipid-core nanocapsules containing BZP for nose-to-brain delivery as an alternative treatment for GBM.

## Materials & methods

### Chemicals

Poly(ε-caprolactone) (PCL, Mn = 10,000 g/mol<sup>-1</sup>, Mw = 14,000 g/mol<sup>-1</sup>, α,ω-hydroxylated), sorbitan monostearate (Span 60) and polysorbate 80 (Tween 80) were obtained from Sigma-Aldrich (MO, USA). Chitosan (Mw = 21 kDa-viscosity 9 cP) was supplied by Primex (Chitoclear FG, deacetylation degree 95%, Siglufjordur, Iceland). Soybean lecithin (Lipoid S75) was obtained from Lipoid (Ludwigshafen, Germany). Caprylic/capric triglyceride was purchased from Delaware (Rio Grande do Sul, Brazil). BZP (521.33 g/mol<sup>-1</sup>) was synthesized and characterized by its melting point, <sup>1</sup>H and <sup>13</sup>C nuclear magnetic resonance, high-resolution mass spectroscopy and elemental analysis in Joaquín María Campos' laboratory (Granada, Spain), as previously published [9]. Dulbecco's modified Eagle's medium (DMEM), fetal bovine serum (FBS), Fungizone, penicillin/streptomycin and 0.5% trypsin/EDTA solution were obtained from Gibco (CA, USA). Propidium iodide (PI), trypan blue and DMSO

and TMZ were obtained from Sigma-Aldrich. AnnexinV-APC and PI were obtained from BD Biosciences (NJ, USA).

### Nanocapsules preparation

LNC formulation was prepared according to the interfacial deposition of the preformed polymer method, as previously described [33]. An organic phase containing PCL (0.1 g), sorbitan monostearate (0.038 g) and caprylic/capric triglyceride (0.16 ml) dissolved in acetone (25 ml) was kept under magnetic stirring at 40°C. In parallel, soybean lecithin (0.08 g) was dissolved in ethanol (5 ml). After complete dissolution of the components, BZP (0.01 g) was added into the organic phase and completely dissolved. The organic phase was injected into 50 ml of an aqueous phase, containing polysorbate 80 (0.08 g), under moderate magnetic stirring. The organic solvents were removed and the suspension was concentrated to a final volume of 9 ml under reduced pressure (rotator evaporator Buchi – RII, Flawil, Switzerland) at 40°C. The final volume was adjusted to 10 ml. Subsequently, chitosan (0.07 g) was solubilized in 1% (v/v) acetic acid aqueous solution (10 ml). The chitosan aqueous solution was filtered (0.45 µm, Merck Millipore, MA, USA) and added dropwise (1 ml) into 9 ml of the formulation. The reaction remained under moderate magnetic stirring for 2 h. This formulation was called BZP-LNC<sup>+</sup>. Blank nanocapsules (LNC<sup>+</sup>) were formulated in the same way but with the omission of BZP. LNC formulations were stored under refrigeration.

### Drug content & encapsulation efficiency

BZP quantification was performed by high-performance liquid chromatography (HPLC-UV, Shimadzu Corporation, Kyoto, Japan) equipped with an LC-20AT pump, SPD-20A detector, CBM-20A controller, LPGE Kit valve and DGU-20A5R degasser. Chromatographic separation was carried out using a column Phenomenex Luna C18 (4.6 × 150 mm, 5 µm) with a mobile phase consisting of acetonitrile: ammonium acetate 20 mM (60:40, v/v, pH 4.0); the flow rate was 1.0 ml·min<sup>-1</sup>. The injection volume was 50 µl and the BZP was detected by UV absorption at 290 nm. Linear calibration curves were obtained in the range of 0.5–20 µg/ml<sup>-1</sup> (R<sup>2</sup> = 0.99). The drug content in the LNC formulations was determined by diluting a nanoparticle suspension (55.6 µl) in the mobile phase (q.s.p. 5 ml). The LNC formulations were then sonicated for 20 min, vortexed for 1 min and filtered through a 0.45 µm membrane (Merck Millipore) before being assayed by HPLC-UV. The encapsulation efficiency (EE) was determined by ultrafiltration-centrifugation using a filter device (30 kDa; Merck Millipore) at 1844× *g* for 20 min (Sigma 1–14 microcentrifuge, Osterode, Germany). EE was calculated using the following formula:

$$\%EE = \frac{C_t - C_f}{C_t} \times 100$$

where EE % is the percentage of the drug that is successfully entrapped into LNCs, *C<sub>t</sub>* is the total concentration of the drug in the formulation and *C<sub>f</sub>* is the concentration of the drug dissolved in the continuous phase (ultrafiltrate).

### Method validation

Following the International Conference on Harmonization (ICH) guidelines, validation was carried out by assessing the following parameters: specificity, linearity, detection and quantification limits, precision (intra- and inter-day), accuracy and robustness [34].

#### Specificity

To evaluate the absence of interferences in the same retention time of BZP, the specificity was evaluated through a comparative analysis between the BZP standard solution, diluted in acetonitrile, LNC<sup>+</sup> and BZP-LNC<sup>+</sup>.

#### Linearity

Linearity was evaluated by constructing a standard curve in the range of 0.5–20 µg/ml<sup>-1</sup>, diluted in acetonitrile: ammonium acetate (60:40 v/v) and prepared from the stock solution of the BZP (500 µg/ml<sup>-1</sup> dissolved in acetonitrile). The linear regression analysis in the concentration range was used to evaluate the linearity of the method. The acceptance criterion for linearity was R<sup>2</sup> = 0.99.

#### Limits of detection & quantification

The limit of detection (LOD) and the limit of quantification (LOQ) were calculated by considering the standard deviation of the intercept of the analytical curve and the slope average of three calibration curves, according to the

following equations:

$$LOD = \frac{(DPa \times 3)}{IC}$$

$$LOQ = \frac{(DPa \times 10)}{IC}$$

where  $DPa$  is the standard deviation of the intercept with the y-axis of three calibration curves,  $IC$  is the slope of the calibration curve.

#### Precision

Precision was assessed in terms of repeatability (intraday) and intermediate precision (interday). Repeatability was calculated from six replicates of the BZP-LNC<sup>+</sup> in a single day. Intermediate precision was evaluated for three replicates of the BZP-LNCs on three days. Precision data were expressed as relative standard deviation percentage (RSD%).

#### Accuracy

Accuracy was carried out in triplicate using samples of LNC<sup>+</sup> spiked with three concentrations (1, 10 and 15 µg/ml<sup>-1</sup>) of BZP solution (500 µg/ml<sup>-1</sup> dissolved in acetonitrile) in the mobile phase. The results were expressed as percent recovery and RSD.

#### Robustness

Robustness was evaluated by slight variations of the chromatographic parameters. Three independent variables at low or high level were investigated: flow rate (0.8 and 1.2 ml·min<sup>-1</sup>), detection wavelength (287 and 293 nm) and mobile phase pH (acetonitrile:ammonium acetate, 60:40; pH 3.5 and 4.5). BZP-LNC<sup>+</sup> at 10 µg/ml<sup>-1</sup> was used for robustness. The estimated variable effects were based on percent recovery and RSD in relation to the standard chromatographic condition (statistically assessed using the one-way analysis of variance). Retention time (min), tailing factor ( $T < 2.0$ ), retention factor ( $K > 2.0$ ) and theoretical plate number ( $N > 2000$ ) were also evaluated.

#### Laser diffraction

Particle size and the size distribution were determined by laser diffraction (Mastersizer 2000, Malvern Instruments, Malvern, UK). The sample was directly added to water in the wet dispersion accessory (Hydro 2000SM-AWM2002, Malvern Instruments) in an amount sufficient to obtain at least 2% obscuration. The particle size was then expressed by using the volume-weighted mean diameter ( $D[4,3]$ ), and the diameters calculated at the 10th, 50th and 90th percentiles ( $D0.1$ ,  $D0.5$  and  $D0.9$ , respectively) of the cumulative size distribution curve, by volume ( $v$ ) and by the number ( $n$ ) of particles. The width of the distribution (Span) was determined according to the following equation:

$$Span = \frac{D0.9 - D0.1}{D0.5}$$

where  $D0.1$ ,  $D0.5$  and  $D0.9$  are the diameters at 10%, 50% and 90% of the cumulative size distribution curve by volume of particles, respectively.

#### Dynamic light scattering

The mean hydrodynamic diameter (z-average diameter) and the polydispersity index (PDI) of the nanocapsules were evaluated by dynamic light scattering (DLS), using a Zetasizer Nano ZS (Malvern Instruments). The samples were diluted 500x in filtered ultrapure water (0.45 µm). The analysis was carried out at 25°C; the light scattering was detected at an angle of 173°, and the z-average diameter and PDI were calculated by the cumulants method.

#### pH & zeta potential

The pH values of BZP-LNC<sup>+</sup> and LNC<sup>+</sup> were determined using a calibrated potentiometer (DM-22 Digimed, São Paulo, Brazil) via direct measurements of the formulations at room temperature. The Zeta potential values

were determined by electrophoretic mobility after the samples were diluted in 10 mmol/l<sup>-1</sup> NaCl aqueous solution (500×), previously filtered (0.45 μm, Millipore, MA, USA) and analyzed by laser Doppler velocimetry (Zetasizer Nano-ZS instrument, Malvern, UK).

### Nanoparticle tracking analysis

Size distribution by the number of particles and particle number density (particles/ml<sup>-1</sup>) were determined by NTA (NanoSight LM10 Instruments, Salisbury, UK). The results were expressed as mean hydrodynamic diameter (Dh), and diameters at percentiles 10, 50 and 90 (D10, D50 and D90, respectively) under the size distribution curves. The samples were diluted in prefiltered ultrapure water (10,000×) and analyzed using a red 635-nm laser. The video clip was captured over 60 s by a CCD camera and processed in NTA 3.2 Analytical Software (dev build 3.2.16). The measurements were performed for three batches.

### Maintenance of cell line

C6 rat glioma, U138 human glioma and MRC-5 human lung fibroblast cell lines were obtained from American Type Culture Collection (ATCC, MD, USA). For the *in vitro* experiments, cells up to 20 passages were grown and maintained in DMEM containing antibiotics (0.5 U/ml<sup>-1</sup> penicillin/streptomycin) and supplemented with 5% (C6 cells) or 10% FBS (U138 and MRC-5) at 37°C in 5% CO<sub>2</sub> humidified atmosphere.

### Preparation & storage of drugs

For the *in vitro* assays, BZP and TMZ were dissolved in DMSO and stored at -20°C. BZP-LNC<sup>+</sup> and LNC<sup>+</sup> were stored under refrigeration (4°C). For each experiment, the stock solutions were further diluted in the respective DMEM for the cells until the desired concentrations were obtained. The final vehicle concentration in cell culture was 0.2% v/v of DMSO or LNC<sup>+</sup>.

### Assessment of glioma cell viability

The cells were seeded in 24-well plates, 10 × 10<sup>3</sup> cells/well (C6 cells) or 20 × 10<sup>3</sup> cells/well (U138 and MRC-5 cells), and 24 h after plating, the GBM cells were treated with 0.1 to 1.0 μM, and the MRC-5 cells were treated with 0.1 to 5 μM of BZP, BZP-LNC<sup>+</sup> or respective vehicles (DMSO or LNC<sup>+</sup>) for 72 h. Cell viability was evaluated using Trypan blue dye exclusion test; after 72 h of treatment, the DMEM was removed from the wells and the cells were washed with PBS (pH 7.4), trypsinized with 0.05% trypsin/EDTA solution and following this, a medium was added (1:2, v/v) and the cell suspensions were diluted with Trypan blue (0.1%). The viable cells (Trypan blue negative) were counted immediately in a Neubauer chamber. The results were expressed as percentage (%) compared with the control. The half-maximal inhibitory concentration (IC<sub>50</sub>) value was determined by the linear theoretical equation ( $y = mx + c$ ), with R<sup>2</sup> > 0.9, based on the cell viability assay.

### Calculation of the combination Index

The cells were seeded in 24-well plates (10 × 10<sup>3</sup> or 20 × 10<sup>3</sup> cells/well, for C6 or U138 cells, respectively), and 24 h after plating, the GBM cells were treated with 0.1–1.0 μM of BZP-LNC<sup>+</sup>, 1–1000 μM of TMZ, association of BZP-LNC<sup>+</sup> plus TMZ 1:1000 or respective vehicles (DMSO or LNC<sup>+</sup>) for 72 h. After treatment, cell viability was evaluated using the Trypan blue dye exclusion test, as described earlier. The results were expressed from the mean values of the fraction affected (Fa) of the three independent experiments.

The effect of drug combinations between BZP-LNC<sup>+</sup> and TMZ in inhibiting cell growth was analyzed by Chou-Talalay equation using CompuSyn 1.0 software (ComboSyn, NJ, USA). The combination index (CI) is a quantitative measure based on the mass-action law of the degree of drug interaction in terms of synergism and antagonism for a given endpoint of the measured effect. CI values < 1.0 are considered synergistic, CI ≥ 1.0 or ≤ 1.1 defines the additive effect, and CI > 1.1 is antagonism, as previously described [35–38]. Dose reduction index (DRI) indicates how many folds of dose reduction are allowed for each drug due to synergism compared with the dose of each drug alone, as already established; DRI = 1, > 1 and < 1 indicates no dose-reduction, favorable dose-reduction and not favorable dose-reduction, respectively [35–38]. IC<sub>50</sub> values, CI and DRI were generated by CompuSyn software.

### Cell cycle analysis

The GBM cells were seeded in 24-well plates ( $10 \times 10^3$  or  $20 \times 10^3$  cells/well, for C6 or U138, respectively), and 24 h after plating, the GBM cells were treated with IC<sub>50</sub> values of BZP, BZP-LNC<sup>+</sup> or respective vehicles for 72 h. At the end of the treatments, the medium and cells were centrifuged at 400x *g* for 6 min. After this, the cells were washed once with phosphate-buffered saline (PBS; pH 7.4), centrifuged and suspended in 300 µl staining solution (0.5 mM Tris-HCl; pH 7.6), 3.5 mM trisodium citrate, 0.1% NP 40 (v/v), 100 µg/ml<sup>-1</sup> RNase and 50 µg/ml<sup>-1</sup> PI) for 15 min in the dark. Data were collected using flow cytometry (FACSCalibur, BD Biosciences) and analyzed using FlowJo 7.6.5 software.

### AnnexinV – APC & PI assay

Apoptotic and/or necrotic cells were quantified using an AnnexinV-APC and PI double-staining kit, in accordance with the manufacturer's instructions (BD Biosciences). The cells were seeded in 24-well plates and treated as described in the previous section. After this, the medium and the cells were harvested and centrifuged at 400x *g* for 6 min. The cells were washed twice with PBS (pH 7.4) and suspended in binding buffer containing APC-conjugated AnnexinV (0.075 µg/ml<sup>-1</sup>) and PI (0.15 µg/ml<sup>-1</sup>). The samples were incubated for 15 min at room temperature in the dark. Data was later collected using flow cytometry (FACSCalibur, BD Biosciences) and analyzed using FlowJo 7.6.5 software. The cells were classified as follows: viable cells (AnnexinV and PI negative; Q1), early apoptotic cells (AnnexinV positive and PI negative; Q2), late apoptotic cells (AnnexinV and PI positive; Q3) or necrotic cells (AnnexinV negative and PI positive; Q4). For quantitative analysis, early apoptosis and late apoptosis were combined and called 'total apoptosis.'

### *In vivo* glioma model

All of the procedures used in the present study followed the Principles of Laboratory Animal Care from the NIH and were approved by the Ethics Committee of the Universidade Federal do Rio Grande do Sul (protocol #337393). Glioma implantation was performed, as previously described [39,40] using 8–9-week-old male Wistar rats (220–300 g). C6 cells at approximately 80% confluence were trypsinized and a total of  $3 \times 10^5$  cells in 3 µl, suspended in medium without FBS, were injected at a depth of 6.0 mm into the right striatum (Bregma coordinates: 0.5 mm posterior and 3.0 mm lateral), using a Hamilton micro-syringe coupled with an infusion pump (1 µl/min<sup>-1</sup>) in rats anesthetized by intraperitoneal administration of 100 mg/kg<sup>-1</sup> ketamine and 10 mg/kg<sup>-1</sup> xylazine). Immediately after surgery, the animals were kept in a warm room until full recovery from the anesthesia.

### Drug preparation for intranasal delivery

The BZP solution was dissolved in 0.9% saline containing 1% methylcellulose, as previously described [11]. TMZ solution (5 mg/ml<sup>-1</sup>) was dissolved in 0.9% saline containing 10% DMSO. BZP-LNC<sup>+</sup> and LNC<sup>+</sup> were aliquoted and stored under refrigeration. At the time of treatment of the animals, all formulations and drugs were at room temperature.

### Animal treatment

Five days after glioma implantation, the animals were randomly divided into six groups (n = seven animals per group), as follows:

- (1) Untreated animals (CTRL group);
- (2) Treated via intranasal with blank nanocapsules (LNC<sup>+</sup>);
- (3) Treated via intranasal with BZP-LNC<sup>+</sup> 44 µg/day<sup>-1</sup> (BZP-LNC<sup>+</sup> group);
- (4) Treated via intranasal with BZP solution 44 µ/day<sup>-1</sup> (BZP group);
- (5) Treated via intraperitoneal with TMZ solution 5 mg/kg/day<sup>-1</sup> (TMZ group);
- (6) Combined treatment with BZP-LNC<sup>+</sup> plus TMZ (TMZ + BZP-LNC<sup>+</sup> group).

The animals were anesthetized with inhaled isoflurane and kept in a supine 45° position (head up) during administration. The free BZP and BZP-LNC<sup>+</sup> were administered intranasally twice a day (22 µg; 25 µl) every 12 h in a total dose of 44 µg (50 µl) per animal per day over 15 consecutive days. TMZ was intraperitoneally administered once a day for 5 consecutive days. After treatment, the rats were decapitated, and the entire brain was removed for volume quantification and the blood was collected for biochemical analyses. As a control, LNC<sup>+</sup> received the same volume of BZP-LNC<sup>+</sup> group.

The animals that received nasal treatment were carefully monitored for signs of distress and discomfort during the procedure (excessive struggling, mucus membrane color changes, ventilatory changes) followed the Principles of Laboratory Animal Care from the NIH and according to project approved by the aforementioned ethics committee.

### Tumor size quantification

For tumor size quantification, four paraffin-fixed tissue sections were stained with hematoxylin and eosin, and the images were captured with a digital camera connected to a microscope (Olympus BX-51, Tokyo, Japan). The tumor area was determined using NHI's ImageJ software. The total volume ( $\text{mm}^3$ ) of the tumor was computed by multiplication of the slice sections (3 mm each) by the tumor areas ( $\text{mm}^2$ ) [39,40].

### Plasma biochemical parameters

The plasma samples were collected to determine the biochemical parameters as markers of toxicity: creatinine, urea, alkaline phosphatase (ALP), creatine phosphokinase (CPK), alanine aminotransferase (ALT) and aspartate aminotransferase (AST). The biochemical experiments were performed in a Cb400i analyzer (Wiener Lab, ARG).

### Statistical analysis

The data were analyzed using GraphPad Prism (version 6.0, GraphPad, CA, USA). The samples presented normal distribution; parametric one-way analysis of variances, followed by a *post hoc* test for multiple comparisons (Tukey test), which was used to measure significance. The statistical significance was set at  $p < 0.05$ .

## Results

### Validation of the analytical method for quantification of BZP-loaded lipid-core nanocapsules

First, the analytical method for the detection and quantification of BZP from LNCs was developed and validated. Specificity was demonstrated by comparing LNC<sup>+</sup> chromatogram with BZP-LNC<sup>+</sup> chromatogram (Figures 1A–C). As expected, the LNC<sup>+</sup> did not show any chromatographic signal in the same retention times of the BZP, demonstrating that the method is specific for drug detection and that there is no interference for the constituents of the nanocapsules formulation. In addition, comparison was made of the BZP-LNC<sup>+</sup> chromatogram with the BZP solution, confirming that the drug retains the same retention time even after being nanoencapsulated (Figures 1B & C).

The linearity of the method was assessed in the concentration range of 0.5–20  $\mu\text{g}/\text{ml}^{-1}$ . The linear equation obtained was  $y = 48574x - 4875$ , and showed an adequate determination coefficient ( $R^2 = 0.99$ ). This revealed that the regression equation was linear ( $F_{\text{calculated}} = 13573.43 > F_{\text{critical}} = 4.96$ ) with no linearity deviation ( $F_{\text{calculated}} = 1.97 < F_{\text{critical}} = 3.71$ ). LOD is determined as the lowest concentration that can be detected by an analytical method but not quantified. LOQ is the lowest concentration that an analytical method can quantify in a sample accurately. In this study, the LOD and LOQ obtained were 0.08  $\mu\text{g}/\text{ml}^{-1}$  and 0.28  $\mu\text{g}/\text{ml}^{-1}$ , respectively.

The repeatability (intraday) and intermediate precision (interday) were measured by the determination of the relative standard deviation percentage. The six repetitions in a single day for the repeatability assay showed values between 95.24 and 99.04%, and RSD was 1.54% (Table 1), demonstrating conformity with the parameters set for the validation of the chromatographic methods for drug quantification. The interday precision values are given in Table 1. All data are lower than the acceptance criterion of 2% [34].

Accuracy was calculated as the percent recovery by the assay of adding a known amount of BZP in LNC<sup>+</sup> to obtain three final concentrations (1, 10 and 15  $\mu\text{g}/\text{ml}^{-1}$ ). Table 1 shows the method accuracy determined by investigating the recovery. The results indicated that recoveries were between 95 and 101% and RSD were 2.00, 0.42 and 0.78% (for 1, 10 and 15  $\mu\text{g}/\text{ml}^{-1}$ , respectively), demonstrating conformity with the limits established by ICH.

The results of the robustness are expressed by percentage of recovery and RSD, obtained using the altered parameters as the pH of the mobile phase, detection wavelength and flow rate. The chromatographic conditions evaluated resulted in small changes in retention time, tailing factor and theoretical plate number compared with the standard chromatographic method. However, no significant differences were observed related to BZP recovery percentage ( $p > 0.05$  and  $\text{RSD} < 2.0$ ), demonstrating the robustness of the method (Table 1).

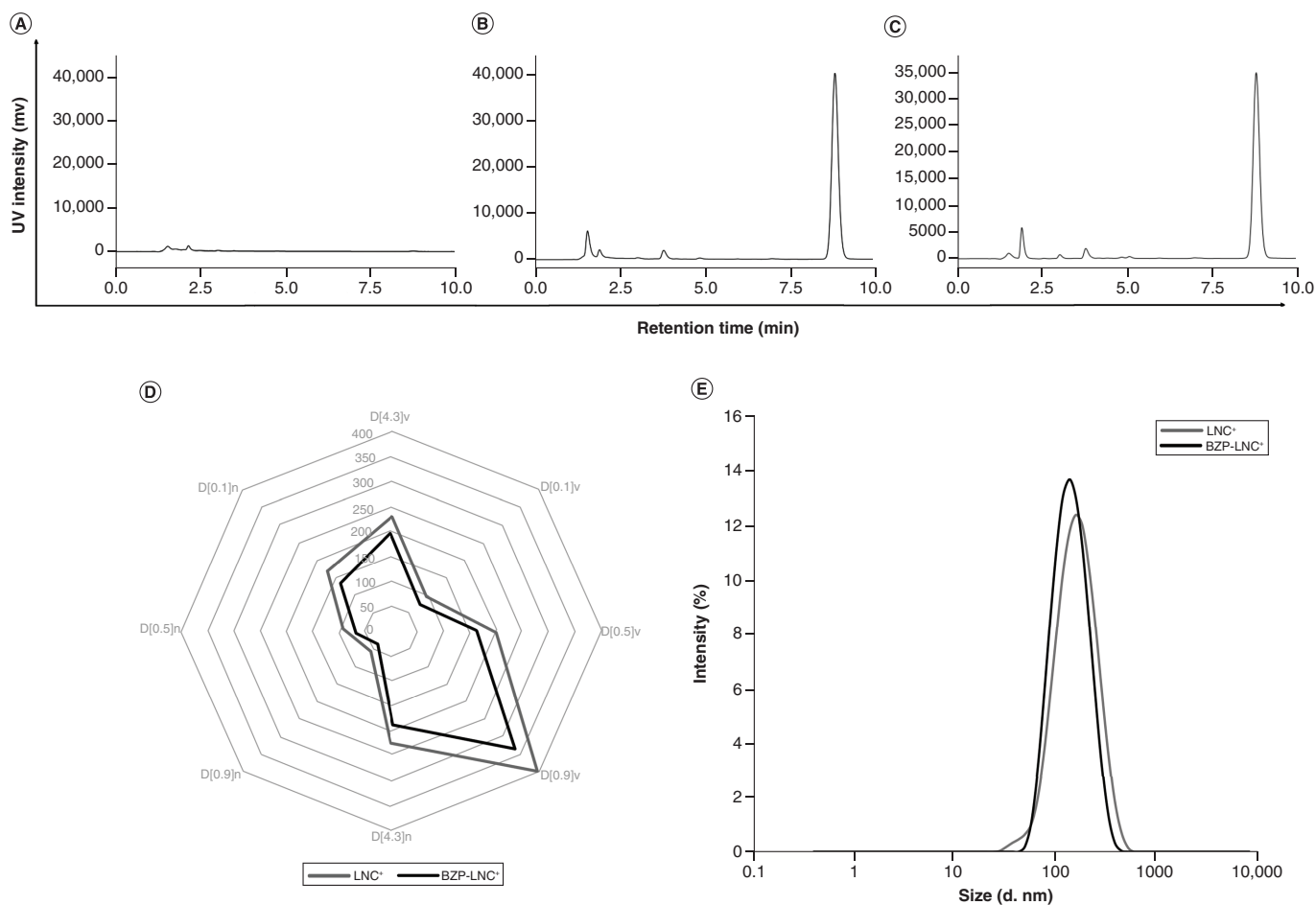


**Figure 1. Nanocapsules characterization.** Representative chromatograms of (A) LNC<sup>+</sup>, (B) bozepinib solution and (C) BZP-LNC<sup>+</sup>. (D) Radar chart presenting the value of volume-weighted mean diameters (D[4,3]) and the mean diameters at percentiles 10, 50 and 90 under the size distribution curves by volume and number of particles. (E) Dynamic light scattering particle size distribution curves for LNC<sup>+</sup> and BZP-LNC<sup>+</sup>. BZP-LNC<sup>+</sup>: Bozepinib-lipid-core nanocapsule; LNC<sup>+</sup>: Lipid-core nanocapsule.

### Characterization of BZP-LNC<sup>+</sup> & LNC<sup>+</sup> formulations

The total BZP content in the nanocapsules (BZP-LNC<sup>+</sup>) was  $0.88 \pm 0.01 \text{ mg/ml}^{-1}$ , with an encapsulation efficiency of 100%. The particle size distribution of BZP-LNC<sup>+</sup> and LNC<sup>+</sup> showed D[4,3] of  $194 \pm 27 \text{ nm}$  (span  $1.54 \pm 0.16$ ) and  $266 \pm 33 \text{ nm}$  (span  $1.49 \pm 0.20$ ), respectively. The values referring to the volume-weighted mean diameters and the diameters at percentiles 10, 50 and 90 (by volume and number) were plotted on the radar chart, which is described as fingerprints of the formulations [41]. As are presented in Figure 1D, the shapes of the radar chart demonstrate narrow size distributions and low polydispersities, as well as the absence of micrometric particles or aggregates.

DLS analysis showed a narrow particle size distribution for both formulations (PDI <0.2) and z-average diameters of  $133 \pm 13 \text{ nm}$  (BZP-LNC<sup>+</sup>) and  $146 \pm 17 \text{ nm}$  (LNC<sup>+</sup>) (Figure 1E). According to the NTA analysis, the hydrodynamic diameter (Dh) varied from  $157 \pm 5$  to  $163 \pm 3 \text{ nm}$  when BZP was added to the formulation. In addition, we compared the light scattered by the LNC<sup>+</sup> formulation with the light scattered by the BZP-LNC<sup>+</sup> formulation (scattered light intensity  $\times$  diameter). The NTA 2D plots (Supplementary Figure 1) show the scattered light spot distributions of the LNC<sup>+</sup> and BZP-LNC<sup>+</sup> samples, which had similar light scattering intensities, indicating the absence of nanocrystals in the formulation. This data indicate an important correlation between the encapsulation mechanism of the drug and its lipophilicity, where the higher is the lipophilicity of the drug, the higher its concentration in the oil core [42]. Because log D of BZP is 4.14 (at pH ranging from 3.0 to 14.0), the drug is mainly distributed in the oil core at saturation concentration in the organic phase.



Table 1. Validation of the method for quantification of bozepinib in lipid-core nanocapsules formulations.

Precision					
Replicates	Intraday precision		Day	Interday precision	
	BZP quantification (%)	RSD (%)		BZP quantification (%)	RSD (%)
1	97.48	1.54	1	97.48 98.49 99.04	0.80
2	98.49				
3	97.36		2	97.52 98.09 100.12	1.39
4	95.68				
5	95.24		3	99.24 97.98 98.24	0.68
6	99.04				
Accuracy					
Concentration ( $\mu\text{g}/\text{ml}^{-1}$ )	Recovery (%)	RSD (%)			
1	95.23 $\pm$ 1.90	1.99			
10	100.90 $\pm$ 0.42	0.42			
15	99.85 $\pm$ 0.77	0.78			
Robustness					
Factor	Rt (min)	N (>2000) mean $\pm$ SD RSD (%)	T (<2.0) mean $\pm$ SD RSD (%)	K (>2.0) mean $\pm$ SD RSD (%)	Recovery (%) mean $\pm$ SD RSD (%)
Normal condition	8.8	9468 $\pm$ 15 (0.2)	1.1 $\pm$ 0 (0)	4.7 $\pm$ 0.01 (0.2)	98.5 $\pm$ 0.5 (0.5)
Flow rate (ml)					
0.8	11.1	9899 $\pm$ 182 (1.8)	1.1 $\pm$ 0.004 (0.4)	4.9 $\pm$ 0.1 (2.0)	95.0 $\pm$ 1.7 (1.8)
1.2	7.5	8284 $\pm$ 54 (0.7)	1.1 $\pm$ 0.001 (0.1)	4.9 $\pm$ 0.01 (0.3)	95.4 $\pm$ 1.8 (1.9)
Wavelength (nm)					
293	9.0	9200 $\pm$ 122 (1.3)	1.1 $\pm$ 0.004 (0.3)	4.9 $\pm$ 0.01 (0.2)	95.3 $\pm$ 1.7 (1.7)
287	9.0	9206 $\pm$ 118 (1.3)	1.1 $\pm$ 0.002 (0.2)	5.0 $\pm$ 0.002 (0.04)	95.2 $\pm$ 1.7 (1.8)
pH					
4.3	9.0	9526 $\pm$ 56 (0.6)	1.1 $\pm$ 0 (0)	5.0 $\pm$ 0.02 (0.4)	97.6 $\pm$ 1.9 (1.9)
3.5	8.8	9455 $\pm$ 42 (0.5)	1.1 $\pm$ 0 (0)	4.9 $\pm$ 0.02 (0.5)	97.2 $\pm$ 1.8 (1.9)

Data are mean  $\pm$  SD of three independent experiments.  
BZP: Bozepinib; K: Retention factor; N: Theoretical plate number; RSD: Relative standard deviation; Rt: Retention time; SD: Standard deviation T: Tailing factor.

The particle number densities for the formulations were  $2.15 \pm 0.36 \times 10^{13}$  (BZP-LNC<sup>+</sup>) and  $2.07 \pm 0.38 \times 10^{13}$  (LNC<sup>+</sup>). The zeta potentials were  $+7.57 \pm 0.68$  mV (LNC<sup>+</sup>) and  $+9.03 \pm 1.99$  mV (BZP-LNC<sup>+</sup>), and the pH showed acid for both formulations,  $3.89 \pm 0.07$  and  $4.04 \pm 0.28$ , for LNC<sup>+</sup> and BZP-LNC<sup>+</sup>, respectively. The results are summarized in Table 2.

### BZP-LNC<sup>+</sup> reduces GBM cell viability interfering with the cell cycle progression & inducing apoptosis

The following step was an evaluation of the BZP-LNC<sup>+</sup> cytotoxicity in the GBM and nontumoral cells using the Trypan blue exclusion method. As shown in Table 3, BZP-LNC<sup>+</sup> reduces GBM cell viability with IC<sub>50</sub> values of  $0.47 \pm 0.03$   $\mu\text{M}$  (C6 cells) and  $0.43 \pm 0.04$   $\mu\text{M}$  (U138 cells), while the BZP solution presents IC<sub>50</sub> values of  $0.50 \pm 0.02$   $\mu\text{M}$  (C6 cells) and  $0.83 \pm 0.02$   $\mu\text{M}$  (U138 cells). Interestingly, BZP-LNC<sup>+</sup> was demonstrated to be more effective in reducing cell growth for the U138 cells when compared with the BZP solution, presenting a significantly lower IC<sub>50</sub> value ( $p = 0.001$ ). In addition, neither blank nanocapsules nor DMSO were able to significantly reduce cell viability, even in the highest concentrations (data not shown).

Furthermore, evaluation was made of the toxicity of the BZP solution and BZP-LNC<sup>+</sup> in MRC-5 nontumoral cells, resulting in IC<sub>50</sub> values significantly greater than the C6 and U138 cells ( $2.49 \pm 0.51$  and  $2.28 \pm 0.55$   $\mu\text{M}$ , for BZP solution and BZP-LNC<sup>+</sup>,  $p = 0.001$ , Table 3). Considering the IC<sub>50</sub> values, the selectivity index *in vitro* (SI) was calculated, which predicts a selective action of the compound, as previously described [43–45]. As shown in Table 3, the C6 cells showed SI values of 4.98 (BZP) and 5.30 (BZP-LNC<sup>+</sup>), and the U138 cells presented

**Table 2. Physicochemical characterization of nanocapsule suspensions.**

Parameter	BZP-LNC <sup>+</sup>	LNC <sup>+</sup>
<b>LD</b>		
D [4.3] (nm)	194 ± 27	266 ± 33
Span	1.54 ± 0.16	1.49 ± 0.20
<b>DLS</b>		
D <sub>h</sub> , z-ave (nm)	133 ± 13	146 ± 17
PDI	0.17 ± 0.03	0.17 ± 0.03
<b>NTA</b>		
D <sub>h</sub> (nm)	163 ± 3	157 ± 5
D <sub>10</sub> (nm)	123 ± 4	121 ± 6
D <sub>50</sub> (nm)	156 ± 3	151 ± 4
D <sub>90</sub> (nm)	222 ± 9	199 ± 1
PND (particles.ml <sup>-1</sup> )	2.15 ± 0.36 × 10 <sup>13</sup>	2.07 ± 0.38 × 10 <sup>13</sup>
Zeta potential (mV)	+9.03 ± 1.99	+7.57 ± 0.68
pH	4.04 ± 0.28	3.89 ± 0.07
Drug content (mg.ml <sup>-1</sup> )	0.88 ± 0.01	–
EE (%)	100%	–

Results are expressed as mean ± standard deviation of three independent experiments.

D10, D50 and D90: Diameter at percentiles 10, 50 and 90, respectively; Dh: Hydrodynamic diameter; Dh, z-ave: z-average hydrodynamic diameter; DLS: Dynamic light scattering; EE: Encapsulation efficiency; LD: Laser diffraction; NTA: Nanoparticle tracking analysis; PDI: Polydispersity index; PND: Particle number density.

**Table 3. IC<sub>50</sub> values of bozepinib solution and BZP-loaded lipid-core nanocapsules in cell lines and *in vitro* SI.**

Cell lines	BZP		BZP-LNC <sup>+</sup>	
	IC <sub>50</sub> ± SD (μM)	SI	IC <sub>50</sub> ± SD (μM)	SI
C6	0.50 ± 0.02	4.98	0.47 ± 0.03	5.30
U138	0.83 ± 0.02	3.00	0.43 ± 0.04 <sup>‡</sup>	4.85
MRC-5	2.49 ± 0.51 <sup>†</sup>	NA	2.28 ± 0.55 <sup>†</sup>	NA

Glioblastoma (GBM) or MRC-5 cells were treated with different concentrations of BZP or BZP-LNC<sup>+</sup> for 72 h. Cell viability was determined by Trypan blue dye exclusion test. IC<sub>50</sub> values was determined by the linear theoretical equation ( $y = mx + c$ ). SI values were calculated from the IC<sub>50</sub> value of the MRC-5/IC<sub>50</sub> value of GBM cells. Data are means ± SD of three independent experiments.

<sup>†</sup>p < 0.001, significantly different from the IC<sub>50</sub> of C6 and U138 cells.

<sup>‡</sup>p < 0.001, significantly different from the IC<sub>50</sub> of BZP-U138 cells.

BZP: Bozepinib; BZP-LNC<sup>+</sup>: Bozepinib-loaded lipid-core nanocapsule; IC<sub>50</sub>: Half-maximal inhibitory concentration; NA: Not applicable; SD: Standard deviation; SI: Selectivity index.

SI = 3.00 (BZP) and SI = 4.85 (BZP-LNC<sup>+</sup>). According to previous studies, SI values  $\geq 3$  are considered selective for cancer cells [46,47].

The percentage of cells at the different phases of the cell cycle (G0/G1, S and G2/M) was analyzed by flow cytometry and demonstrated in Figures 2A & B. BZP-LNC<sup>+</sup> was able to induce cell cycle arrest in the S phase of the U138 cells from 25.99 to 31.75% (p = 0.0001) while reducing the cells in the G0/G1 phase from 55.91 to 50.26% (p = 0.0060), compared with the LNC<sup>+</sup>. On the other hand, there were no statistical differences in the cell cycle progression in the C6 cell lines.

After this, evaluation was made of the cytotoxic parameters related to cell death after BZP or BZP-LNC<sup>+</sup> treatment. Apoptosis-inducing effect was performed by annexin V and PI assay after 72 h of treatment. Double staining with annexin V and PI provides a sensitive method to detect the stages of cell death resulting from apoptotic and/or necrotic processes. In this assay, viable or cells without measurable apoptosis, where the cell membranes are intact, remain negative for annexin V and PI; cells that are in the stage of cell death from early apoptosis are annexin V positive and PI negative; cells in the final stage of apoptosis (late apoptosis) are positive for both annexin V and PI. Cells in necrotic death, which have damaged and permeable cell membranes, remain PI positive only. The percentage of cells positive for annexin V in both early and late apoptosis stages are plotted in this study as cells in total apoptosis. BZP-LNC<sup>+</sup> significantly increased the induction of total apoptosis when compared to the BZP solution in the C6 cells, from 8.31 (BZP) to 20.03% (BZP-LNC<sup>+</sup>) (p = 0.0001, Figures 2C & D), and the U138 cells also presented significantly higher levels of apoptosis after BZP-LNC<sup>+</sup> treatment, from 10.8 (BZP) to 16.62% (BZP-LNC<sup>+</sup>) (p = 0.0001, Figures 2E & F). In contrast, the BZP solution significantly increased the percentage of necrotic C6 cells compared with BZP-LNC<sup>+</sup>, 4.83 (BZP) versus 1.37% (BZP-LNC<sup>+</sup>), p = 0.0001.

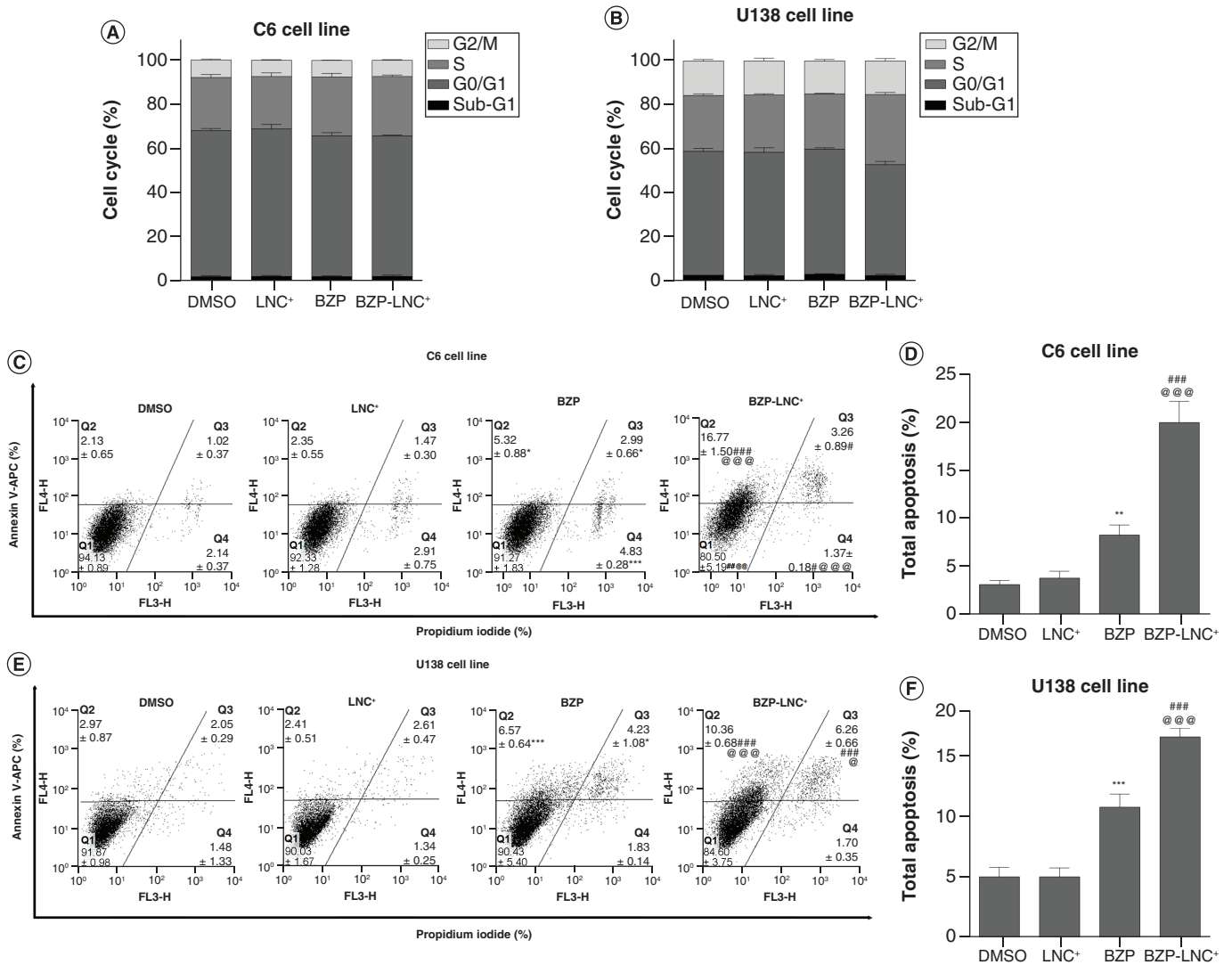


**Figure 2.** Glioblastoma cells were treated with different concentrations of bozepinib (BZP) solution or BZP-loaded lipid-core nanocapsules (BZP-LNC<sup>+</sup>) for 72 h. (A) Quantitative cell cycle analysis in C6 cells. (B) Quantitative cell cycle analysis in U138 cells. (C) Dot-plot (Q1 = viable cells, Q2 = early apoptosis, Q3 = late apoptosis and Q4 = necrosis) and (D) quantitative analysis of total apoptosis (%) in C6 cells. (E) Dot-plot (Q1 = viable cells, Q2 = early apoptosis, Q3 = late apoptosis and Q4 = necrosis) and (F) quantitative analysis of total apoptosis (%) in U138 cells. Data are presented as means ± standard deviation of three independent experiments. \*p < 0.05; \*\*p < 0.01 and \*\*\*p < 0.001: significantly different from DMSO. #p < 0.05; ##p < 0.01 and ###p < 0.001: significantly different from LNC<sup>+</sup>. @p < 0.05, @@p < 0.01 and @@@p < 0.001: significantly different between BZP solution and BZP-LNC<sup>+</sup>. BZP: Bozepinib; BZP-LNC<sup>+</sup>: Bozepinib-loaded lipid-core nanocapsule; LNC<sup>+</sup>: Lipid-core nanocapsule.

It should be highlighted that BZP-LNC<sup>+</sup> might induce apoptosis instead necrosis possible due to a sustained and time-dependent release, whereas free BZP, without any releasing control, might trigger necrotic cell death in a small subset of susceptible cells, considering cells' plasticity. Additionally, the controls (LNC<sup>+</sup> and DMSO) did not show significantly relevant apoptosis induction in both the GBM cells (p = 0.2316 and p = 0.9999 for C6 and U138 cells, respectively).

### Synergistic effects of TMZ plus BZP-LNC<sup>+</sup> in GBM cells

To explore the possibility of synergistic cytotoxicity, GBM cells were treated with different concentrations of BZP-LNC<sup>+</sup> and TMZ, either alone or in combination. Analysis was performed using CompuSyn software, based on the unified theory of the median-effect equation of the mass-action law and the combination index theorem [35–38]. As shown in Table 4, BZP-LNC<sup>+</sup> maintained its IC<sub>50</sub> values, even when calculated with different methodologies (linear

**Table 4. Combination of bozepinib-loaded lipid-core nanocapsules and temozolomide against glioblastoma cell growth.**

Compound	IC <sub>50</sub> ± SD (μM)	CI	DRI
<b>C6 cell line</b>			
BZP-LNC <sup>+</sup>	0.46 ± 0.06	NA	2.48 ± 0.25
TMZ	528.7 ± 19.17	NA	2.92 ± 0.56
BZP-LNC <sup>+</sup> + TMZ	0.14 ± 0.02 + 186.2 ± 35.86	0.75 ± 0.10	NA
<b>U138 cell line</b>			
BZP-LNC <sup>+</sup>	0.42 ± 0.09	NA	2.42 ± 0.55
TMZ	737.5 ± 58.98	NA	3.38 ± 0.25
BZP-LNC <sup>+</sup> + TMZ	0.17 ± 0.01 + 217.8 ± 2.28	0.72 ± 0.12	NA

Cell viability was determined by the Trypan blue dye exclusion test after glioblastoma cells were treated with different concentrations of drugs for 72 h. IC<sub>50</sub>, CI and DRI were obtained by CompuSyn software. Data are presented as the mean ± SD of three independent experiments.

BZP-LNC<sup>+</sup>: Bozepinib-loaded lipid-core nanocapsule; CI: Combination index; DRI: Dose-reduction index; IC<sub>50</sub>: Half-maximal inhibitory concentration; NA: Not applicable; SD: Standard deviation; TMZ: Temozolomide.

theoretical equation, as shown in Table 3, or Chou–Talalay equation analyzed by CompuSyn software). In addition, it is worth noting that the IC<sub>50</sub> was much higher for the TMZ; the C6 cells presented IC<sub>50</sub> of 528.7 ± 19.17 μM and the U138 cells showed an IC<sub>50</sub> of 737.5 ± 58.98. Curiously, the combination of BZP-LNC<sup>+</sup> and TMZ led to a significantly enhanced killing effect compared with the single-agent treatments, reducing the IC<sub>50</sub> value by more than half. These results suggest that the combination of these drugs produced an explicit synergistic effect with CI value <1 (0.75 ± 0.10 for C6 cells and 0.72 ± 0.12 for U138 cells), a quantitative definition for synergism (Table 4 & Figures 3A & D). The synergistic effect was also investigated using the isobologram, which consists of a graphical representation of the interaction of two drugs that exhibit similar effects in equipotent pairs for a given level of inhibition. In the isobologram, synergism is represented by the treatment combination (symbol) below its respective Fa isobole (line) [36]. As shown in Figure 3B & E, the combination of TMZ plus BZP-LNC<sup>+</sup> results in a synergistic effect for 50% inhibition of cells (Fa 0.5), 75% (Fa 0.75) and 90% (Fa 0.9). The analysis of the DRI, which measures the number of folds a drug concentration can be reduced in combination, demonstrated a reduction of approximately 2.5-fold in the TMZ and BZP-LNC<sup>+</sup> concentrations, indicating a favorable drug combination (Table 4 & Figures 3C & F).

After validating the theoretical reduction of the TMZ and BZP-LNC concentrations, evaluation was made of the cytotoxic parameters related to cell death after cotreatment with BZP-LNC<sup>+</sup> (0.14 or 0.17 μM, for C6 or U138 respectively) plus TMZ (186 or 217 μM, for C6 or U138, respectively) by annexin V and PI, followed by flow cytometry analysis after 72 h of treatment. Again, BZP-LNC<sup>+</sup> alone significantly induced apoptosis in the GBM cells compared with the vehicles (represented by the association of vehicles used in the study, DMSO plus LNC<sup>+</sup>), from 2.42 to 17.45% in the C6 cells (p = 0.0007) and from 5.84 to 17.85% in the U138 cells (p = 0.0001). Furthermore, TMZ was also able to significantly induce total apoptosis by approximately 10-fold and 5-fold, compared with the vehicle, for the C6 and U138 cells, respectively (p = 0.0001); as expected, the combination of BZP-LNC<sup>+</sup> plus TMZ led to a significant enhancement in the percentage of apoptotic GBM cells, from 2.42 to 31.09%, in the C6 cells (p = 0.0001, Figures 3G & H), and from 5.84 to 24.30%, in the U138 cells (p = 0.0001, Figures 3I & J). Collectively, these results suggest that combinatory treatment between BZP-LNC<sup>+</sup> and TMZ improves the cytotoxic effect of these compounds against GBM cells.

### Combined treatment with TMZ & BZP-LNC<sup>+</sup> has synergistic effects by reducing the tumor size in a rat glioma model

To evaluate the *in vivo* antitumor activity of BZP-LNC<sup>+</sup> and TMZ, either alone or in combination, a rat glioma model was established by injecting glioma cells into the rat brain. After 5 days of tumor growth and 15 days of treatment, the brain was removed and the tumor size evaluated (Figure 4A). Intranasal treatment of the animals bearing glioma with BZP-LNC<sup>+</sup> alone resulted in a 42.32% reduction in the tumor volume in comparison with the LNC<sup>+</sup> treatment (from 87.79 ± 11.25 to 50.64 ± 17.73 mm<sup>3</sup>, p = 0.0007), whereas intraperitoneal treatment with TMZ alone reduced the tumor size by 53.29% compared with the CTRL group (from 91.65 ± 15.05 to

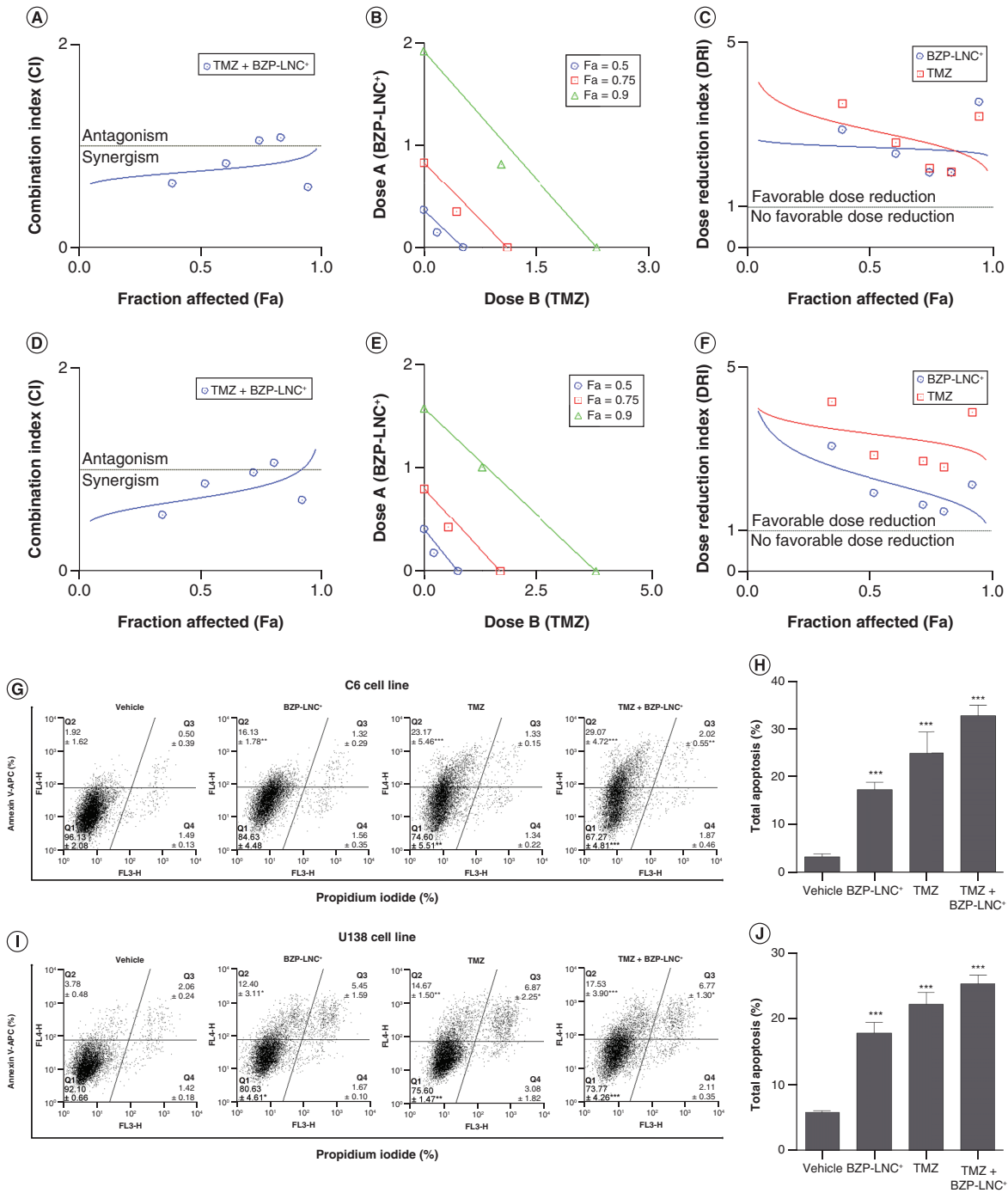


**Figure 3. Representative graphics for BZP-LNC<sup>+</sup>, TMZ and TMZ + BZP-LNC<sup>+</sup> treatments in glioblastoma cells after 72 h. (A) Fa-CI plot, (B) isobologram and (C) Fa-DRI plot in C6 cells. (D) Fa-CI plot, (E) isobologram and (F) Fa-DRI plot in U138 cells. (G) Dot-plot (Q1 = viable cells, Q2 = early apoptosis, Q3 = late apoptosis and Q4 = necrosis) and (H) quantitative analysis of total apoptosis (%) in C6 cell line. (I) Dot-plot (Q1 = viable cells, Q2 = early apoptosis, Q3 = late apoptosis and Q4 = necrosis) and (J) quantitative analysis of total apoptosis (%) in U138 cell line. Vehicle was represented by the cotreatment with DMSO plus LNC<sup>+</sup>. Data are presented as means ± standard deviation of three independent experiments.**

\*p < 0.05; \*\*p < 0.01; \*\*\*p < 0.001; significantly different from vehicle.

BZP-LNC<sup>+</sup>: Bozepinib-loaded lipid-core nanocapsule; CI: Combination index; DRI: Dose-reduction index; Fa: Fraction affected; Fa = 0.5 (50% of cell proliferation inhibition); Fa = 0.75 (75% of cell proliferation inhibition); Fa = 0.9 (90% of cell proliferation inhibition); TMZ: Temozolomide.

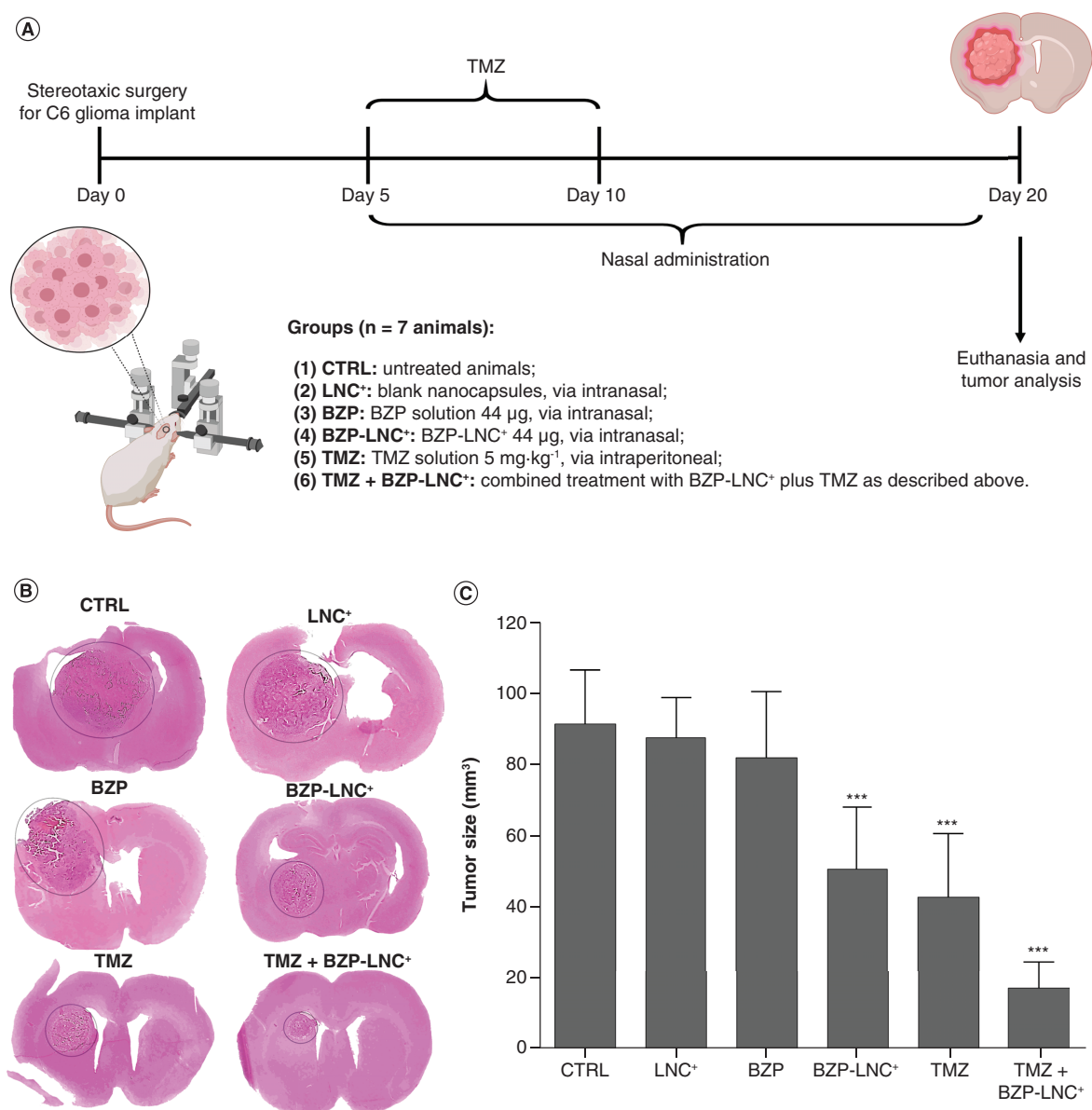


**Figure 4. Cotreatment with TMZ and BZP-LNC<sup>+</sup> reduces tumor size, demonstrating a potent synergistic effect. (A)** Timeline of the experiment and therapeutic scheme employed **(B)** Representative tumor images and **(C)** tumor size quantification of implanted gliomas. The values were represented as means ± standard deviation of seven animals per group.

\*\*\*p < 0.001: significantly different from the CTRL.

BZP-LNC<sup>+</sup>: Bozepinib-loaded lipid-core nanocapsule; CTRL: Control; LNC<sup>+</sup>: Lipid-core nanocapsule; TMZ: Temozolomide.

42.81 ± 17.75 mm<sup>3</sup>, p = 0.0001). In contrast, the difference in the tumor size between the TMZ plus BZP-LNC<sup>+</sup> and the CTRL rats was 81.16% (from 91.65 ± 15.05 to 17.27 ± 7.29 mm<sup>3</sup>, p = 0.0001) (Figures 4B & C). The tumor size of the untreated animals was at the same magnitude of the LNC<sup>+</sup> and the BZP-treated groups (Figures 4B & C).

Assessment was also made of the possible cytotoxic effects of treatment with BZP-LNC<sup>+</sup> or TMZ + BZP-LNC<sup>+</sup> on rats. After 15 days of treatment (20 days after C6 cells implantation), blood was drawn, and the following biochemical parameters were analyzed: creatinine, urea, alkaline phosphatase, creatine phosphokinase, alanine aminotransferase and aspartate aminotransferase to assess hepatic and renal function. As shown in [Supplementary](#)

Table 1, the treatments used in this study did not alter the biochemical parameters in the rats, compared with the CTRL group.

## Discussion

The current study presents a novel lipid-core nanocapsules formulation of BZP for nose-to-brain delivery, which was successfully developed, characterized and investigated against GBM.

The proposed HPLC-UV method was validated in terms of specificity, linearity, accuracy, precision and robustness in accordance with ICH guidelines [34]. The results obtained were within the acceptable ranges, and this method provides an adequate retention time to ensure efficient separation and facilitate routine analysis. Considering that the formulation characteristics, BZP-LNC<sup>+</sup> presented some strategies for increasing brain bioavailability after nose-to-brain delivery, such as the presence of a surfactant, coating the surface with chitosan and appropriate nano-size and zeta potential.

Studies demonstrate that the presence of surfactants such as polysorbate 80 is today the gold standard for increasing the BBB crossover of NPs as they have been shown to increase apolipoprotein–NP interaction, playing a similar role to target ligands, allowing NPs to be captured by receptor-mediated transport. Moreover, they are able to inhibit efflux transporters such as P-glycoproteins [48–51]. Another strategy to reach the CNS is to coat the surface of the nanocapsules with specific ligands [51]. Chitosan-coated NPs have been shown to increase the efficiency of targeting the brain, improving the therapeutic potential of drugs [52–54]. In addition, chitosan can increase or reverse the zeta potential of the nanoparticle to positive, which can confer a greater biological interaction with anionic cell barriers, increasing cell internalization [54]. Therefore, chitosan can control the release, adhere to the mucus and open the hermetic junctions of the nasal membrane, which favor its application by nose-to-brain delivery [55]. In addition, the positive zeta potential may have an important impact on the interaction between NPs and tumor tissue [51]. According to some published studies, the negative charges on tumor cell membranes can potentiate the electrostatic interaction with positively charged NPs, being trapped in the tumor for a longer period, compared with neutral or negatively charged particles [56,57]. In this same sense, NPs with a diameter between 10–200 nm exhibit higher BBB penetration and allow passive accumulation in brain tumors, inducing a more efficient therapeutic effect by the enhanced permeability and retention, which is responsible for the selective targeting and the accumulation of drugs in tumor tissue much more than they do in normal tissue [58,59].

The LNCs were formulated by interfacial deposition using the preformed polymer method, and all the formulations showed adequate nanotechnological characteristics (particle size  $194 \pm 27$  nm, polydispersity index  $<0.2$ ) and high encapsulation efficiency (100%). In this sense, we have successfully demonstrated that BZP-LNC<sup>+</sup> was designed using all the strategies mentioned for nose-to-brain delivery. A limitation of this work is that we did not analyze the LNC formulations by scanning electron microscopy (SEM) or transmission electron microscopy (TEM) or perform long-term stability. However, in previous studies from our laboratory, we have analyzed different LNC formulations by SEM and/or TEM, ensuring that the mean hydrodynamic diameter and PDI correlates with quality standards in SEM/TEM [60–64]. Importantly, to be sure that formulations were adequate for biological evaluation, we analyzed mean hydrodynamic diameter, PDI, drug content and encapsulation efficiency before cells and animals' treatment.

The following step was evaluation of the cytotoxic effect of BZP-LNC<sup>+</sup> in GBM cell lines and nontumor cell lines. A decrease in GBM cell growth after BZP-LNC<sup>+</sup> treatment was observed, with significantly lower IC<sub>50</sub> values compared with the MRC-5 cells, thus demonstrating a selective action for cancer cells by presenting an SI  $\geq 3$  [46,47]. Furthermore, BZP-LNC<sup>+</sup> was demonstrated to be more effective in reducing GBM cell viability than the BZP solution after 72 h. Thus, these results provide evidence that the compound is effectively being released from the LNCs and is being able to exert its effect compared with free BZP. Regarding cell death induction, BZP-LNC<sup>+</sup> significantly increased the percentage of total apoptosis (early and late apoptotic cells), approximately 2.5-fold (C6 cells) and 1.5-fold (U138 cells) compared with the BZP solution. The greater extent of apoptosis, which is more desirable than necrosis in oncotherapy, may reflect a possible sustained release of BZP when nanoencapsulated.

Drug combinations have gained great attention in recent years because they offer the advantage of synergistic antitumor activity at relatively lower concentrations of each drug, reducing possible side effects and minimizing or delaying resistance induction associated with GBM treatment [65,66]. Therefore, an evaluation has been made of the effect of combined treatment between TMZ, the current gold therapy for GBM, and BZP-LNC<sup>+</sup> through Compusyn software. Both the Fa-CI plot, which is an effect-oriented graphic, and the isobologram, which is a dose-oriented graphic, showed exactly the same results – that is, a synergistic effect for the combination TMZ-BZP-

LNC<sup>+</sup>. Again, the CI values indicated a synergistic cytotoxic effect *in vitro* because they were less than one [35–38]. Another relevant result is the DRI, which indicates how much each concentration can be reduced, in a synergistic combination, to provide the same effect as appears in an isolated form [35–38]. The results show that the concentration used for TMZ and BZP-LNC<sup>+</sup> can be reduced approximately 2.5-fold when used in combination to produce the same effect compared with the single agents. Given the synergistic effect by the combined treatment with TMZ plus BZP-LNC<sup>+</sup>, evaluation was made of an interaction between these drugs in the induction of apoptosis and/or necrosis in GBM cells. Although treatment with TMZ or BZP-LNC<sup>+</sup> alone increased the percentage of apoptotic cells, a combination of both drugs (TMZ + BZP-LNC<sup>+</sup>), approximately 2.5-fold less concentrated, significantly increased apoptotic cells, confirming the *in vitro* synergistic effect.

As a follow-up, evaluation was made of the *in vivo* antiglioma activity of BZP-LNC<sup>+</sup> alone and in cotreatment with TMZ (TMZ + BZP-LNC<sup>+</sup>). In addition to using the strategies already mentioned to increase the BZP's capacity to reach the CNS, a less invasive administration tool was chosen, the intranasal route. The nose-to-brain route has attracted much attention in recent years due to its innovative way of overcoming the BBB [30,67,68]. After reaching the nasal cavity, a drug-loaded internal nanocarrier can be transported along with the olfactory bulb (olfactory route) and trigeminal nerve (trigeminal route) directly to the CNS, increasing drug absorption and promoting BBB bypass with fewer systemic adverse effects [32,69].

In the first set of *in vivo* experiments, we conducted a pilot study to evaluate the effect of nanocapsules on a limited number of animals and groups (without LNC and BZP groups). In the therapeutic scheme presented in [Supplementary Figure 2A](#), 8 days after C6 cell implantation, treatment was initiated with a daily application of 100 µl intranasally (50 µl in each nostril) of BZP-LNC<sup>+</sup>. Previously published studies suggest that the optimal volume for nasal administration ranges from 20 to 100 µl [70–73]. In this context, we first opted to evaluate the effect of nasal administration with 88 µg BZP-LNC<sup>+</sup> (100 µl). Surprisingly, after intranasal treatment, the rats' lungs showed visible morphological lesions compared with those that did not receive the formulation, indicating a possible toxicity after intranasal treatment and inconsistent brain drug delivery with nonsignificant reduction in tumor size following BZP-LNC<sup>+</sup> treatment ([Supplementary Figure 2B & C](#)). Although we used the recommended nasal administration volume from previous studies, there are relatively few reports on the ideal administration conditions and established dosing regimens, such as volume, time periods and administration speed. In addition, studies comparing lung toxicity after intranasal delivery of staggered volumes are rare [70–73]. Of note, even with lung toxicity, biochemical analyses showed no difference among the treatments and the control group ([Supplementary Table 2](#)). Furthermore, it is important to note that neither LNCs nor LNCs carrying various drugs demonstrated lung or nasal toxicity after nasal administration [30,74–77].

In view of this, a decision was made to reduce the volume of intranasally administered formulations. Previous studies demonstrated that after 3–5 days of C6 cell implantation, it was already possible to see intracranial tumor formation [78–80]. After 5 days of C6 cell implantation, treatment was initiated with two daily applications of 12.5 µl in each nostril, totaling 50 µl per day, as stated in the Materials & Methods section. In this condition, BZP-LNC<sup>+</sup> or TMZ antiglioma effect was significantly greater than free-BZP or the control group. In addition, the antitumor effect of the association of TMZ and BZP-LNC<sup>+</sup> resulted in a remarkable reduction in glioma size, approximately 81% compared with the control group ( $p = 0.0001$ ), confirming the synergistic antiglioma efficacy of BZP-LNC<sup>+</sup> plus TMZ. There were no visible changes in organs such as lungs, liver and kidneys (data not shown), and there were no changes in the biochemical analyses ([Supplementary Table 1](#)).

### Conclusion & future perspective

We have developed a simple, rapid and sensitive analytical method to quantify BZP-loaded LNCs, a promising compound for GBM treatment. We have developed a formulation containing chitosan-coated LNCs, which showed high encapsulation efficiency for BZP, adequate mean particle sizes (<200 nm) and narrow size distribution. BZP-LNC<sup>+</sup> promoted cytotoxicity effects against GBM cell lines with low IC<sub>50</sub> values, inducing cell apoptosis in C6 and U138 cells. Further, combined BZP-LNC<sup>+</sup> and TMZ treatment showed a synergistic cytotoxic effect in GBM cells, potentiating the apoptosis induction, and even reducing 2.5-fold the concentration of both drugs tested. The cotreatment with TMZ + BZP-LNC<sup>+</sup> reduced the *in vivo* glioma growth by approximately 81% compared with the control group.

To further enhance the synergistic effects between BZP-LNC and TMZ, different types of administration and concentrations of these combined therapies should be tested to maximize the synergistic antitumor effect and ensure a safe and nontoxic therapeutic regimen. Furthermore, additional nanocapsules characterization studies such as



TEM and/or SEM and stability studies need to be evaluated to ensure shelf-life formulation validity. Additionally, in-depth studies of the synergistic antitumor effect and its mechanism of action between BZP-LNC<sup>+</sup> and TMZ should be performed in *in vivo* experiments. Finally, the present study provides an initial basis for the use of cotreatment with TMZ and BZP-LNC<sup>+</sup> in GBM therapy as a first step toward eventual clinical application.

### Summary points

- Anticancer drug-loaded nanocapsules are promising tools for glioblastoma (GBM) treatment.
- This study has aimed at developing an innovative formulation containing bozepinib-loaded lipid-core nanocapsules (BZP-LNC<sup>+</sup>).
- The analytical method of quantifying BZP in nanocapsules using high-performance liquid chromatography has been shown to be sensitive and effective.
- The nanocapsules showed high encapsulation efficiency, adequate particle sizes and narrow size distribution.
- BZP-LNC<sup>+</sup> exert antitumor activity in GBM cells inducing cell death by apoptosis.
- Cotreatment between BZP-LNC<sup>+</sup> and TMZ showed a synergistic cytotoxic effect in GBM cells, potentiating apoptosis induction.
- *In vivo* rat GBM model showed that TMZ plus BZP-LNC<sup>+</sup> significantly inhibited tumor growth.

### Supplementary data

To view the supplementary data that accompany this paper please visit the journal website at: [www.futuremedicine.com/doi/suppl/10.2217/nnm-2021-0164](http://www.futuremedicine.com/doi/suppl/10.2217/nnm-2021-0164)

### Author contributions

AF Dias was responsible for the conception and design of this study; acquisition, analysis and interpretation of *in vitro* data; *in vivo* glioma model and treatment of animals; interpretation of data and also writing the manuscript. DR Dallemole and FA Bruinsmann were responsible for validation and characterization of lipid-core nanocapsules. LFL Silva contributed to *in vivo* glioma model; AR Pohlmann and SS Guterres developed lipid-core nanocapsule formulations, contributed to ideas throughout the process and revised the final draft. O Cruz-López and A Conejo-García were involved in the synthesis of bozepinib. JM Campos kindly donated bozepinib for this study and revised the final draft. AMO Battastini supported the work financially and revised the final draft. F Figueiró was responsible for the design and drafting of this study, critical revision and final approval of the version to be published.

### Acknowledgments

The authors thank the following Brazilian agencies that supported this study: Conselho Nacional de Desenvolvimento Científico e Tecnológico (CNPq), Coordenação de Aperfeiçoamento de Pessoal de Nível Superior (CAPES) and Fundação de Amparo à Pesquisa do Estado do Rio Grande do Sul (FAPERGS).

### Financial & competing interests disclosure

This study is supported by CNPq (AF Dias fellowship and CNPq/PQ no. 302879/2017-0, AMO Battastini grant), FAPERGS (FAPERGS/PQG grant no. 19/2551-0001783-9; ARD grant no. 19/2551-0001269-1 and PRONEX no. 16-2551-0000467-6) and INCT/CNPq/CAPES/FAPERGS grant no. 465671/2014-4). The authors have no other relevant affiliations or financial involvement with any organization or entity with a financial interest in or financial conflict with the subject matter or materials discussed in the manuscript apart from those disclosed.

Writing support was provided by Philip White and was funded by CNPq.

### Ethical conduct of research

The authors state that they have obtained appropriate institutional review board approval or have followed the principles outlined in the Declaration of Helsinki for all human or animal experimental investigations.

### Data sharing statement

The data that support the findings of this study are available from the corresponding author, upon reasonable request.

## References

Papers of special note have been highlighted as: ● of interest; ●● of considerable interest

1. McFaline-Figueroa JR, Lee EQ. Brain tumors. *Am. J. Med.* 131(8), 874–882 (2018).
2. Stupp R, Mason WP, van den Bent MJ *et al.* Radiotherapy plus concomitant and adjuvant temozolomide for glioblastoma. *N. Engl. J. Med.* 352(10), 987–996 (2005).
3. Jiapaer S, Furuta T, Tanaka S *et al.* Potential strategies overcoming the temozolomide resistance for glioblastoma. *Neurol. Med. Chir.* 58(10), 405–421 (2018).
4. Wen PY, Kesari S. Malignant gliomas in adults. *N. Engl. J. Med.* 359(5), 492–507 (2008).
5. Chen J, Li Y, Yu TS *et al.* A restricted cell population propagates glioblastoma growth after chemotherapy. *Nature.* 488(7412), 522–526 (2012).
6. Stupp R, Taillibert S, Kanner A *et al.* Effect of tumor-treating fields plus maintenance temozolomide vs maintenance temozolomide alone on survival in patients with glioblastoma: a randomized clinical trial. *JAMA* 318(23), 2306–2316 (2017).
7. Stupp R, Brada M, van den Bent MJ *et al.* High-grade glioma: ESMO Clinical Practice Guidelines for diagnosis, treatment and follow-up. *Ann. Oncol.* 25(3), 93–101 (2014).
8. Kortmann RD, Jeremic B, Weller M *et al.* Radiochemotherapy of malignant glioma in adults. Clinical experiences. *Strahlenther. Onkol.* 179(4), 219–232 (2003).
9. López-Cara LC, Conejo-García A, Marchal JA *et al.* New (RS)-benzoxazepin-purines with antitumor activity: the chiral switch from (RS)-2,6-Dichloro-9-[1-(*p*-nitrobenzenesulfonyl)-1,2,3,5-tetrahydro-4,1-benzoxazepin-3-yl]-9*H*-purine. *Eur. J. Med. Chem.* 46(1), 249–258 (2011).
10. Marchal JA, Carrasco E, Ramírez A *et al.* Bozepinib, a novel small antitumour agent, induces PKR-mediated apoptosis and synergizes with IFN $\alpha$  triggering apoptosis, autophagy and senescence. *Drug Des. Devel. Ther.* 7, 1301–1313 (2013).
11. Ramírez A, Boulaiz H, Morata-Tarifa C *et al.* HER2-signaling pathway, JNK and ERKs kinases, and cancer stem like cells are targets of bozepinib small compound. *Oncotarget.* 5(11), 3590–3606 (2014).
- **Paper that shows that *in vitro* cytotoxicity and *in vivo* anticancer efficacy of bozepinib.**
12. Dias AdF, Scholl JN, Moritz CEJ *et al.* New insights into cytotoxic mechanisms of bozepinib against glioblastoma. *Eur. J. Pharm. Sci.* 162:105823 (2021).
- **Demonstrates *in vitro* bozepinib cytotoxicity against glioblastoma.**
13. Atkinson F, Cole S, Green C, van de Waterbeemd H. Lipophilicity and other parameters affecting brain penetration. *Curr. Med. Chem.* 2(3), 229–240 (2002).
14. Pajouhesh H, Lenz GR. Medicinal chemical properties of successful central nervous system drugs. *NeuroRx.* 2(4), 541–553 (2005).
- **Paper that discusses fundamental physiochemical features of CNS drugs to penetrate the blood–brain barrier and exhibit CNS activity.**
15. van de Waterbeemd H, Camenisch G, Folkers G *et al.* Estimation of blood-brain barrier crossing of drugs using molecular size and shape, and H-bonding descriptors. *J. Drug Target.* 6(2), 151–165 (1998).
16. Pardridge WM. CNS drug design based on principles of blood-brain barrier transport. *J. Neurochem.* 70(5), 1781–1792 (1998).
17. Kelder J, Grootenhuis PD, Bayada DM *et al.* Polar molecular surface as a dominating determinant for oral absorption and brain penetration of drugs. *Pharm. Res.* 16(10), 1514–1519 (1999).
18. Feng MR. Assessment of blood–brain barrier penetration: in silico, in vitro and in vivo. *Curr. Drug Metab.* 3(6), 647–657 (2002).
19. Zhao M, van Straten D, Broekman MLD *et al.* Nanocarrier-based drug combination therapy for glioblastoma. *Theranostics* 10(3), 1355–1372 (2020).
20. Erdoğar N, Safiye A, Bilensoy E. Nanocapsules for drug delivery: an updated review of the last decade. *Recent Pat. Drug Deliv. Formul.* 12(4), 252–266 (2018).
21. Aparicio-Blanco J, Torres-Suárez AI. Glioblastoma multiforme and lipid nanocapsules: a review. *J. Biomed. Nanotechnol.* 11(8), 1283–311 (2015).
22. Venturini CG, Jäger E, Oliveira CP *et al.* Formulation of lipid core nanocapsules. *Colloids Surf. A Physicochem. Eng. Asp.* 375, 200–208 (2011).
23. Battaglia L, Gallarate M. Lipid nanoparticles: state of the art, new preparation methods and challenges in drug delivery. *Expert Opin. Drug Deliv.* 9(5), 497–508 (2012).
24. Thamrook S, Subhi SS, Savitha SK, Mathan M. Applications of lipid core nanocapsules: novel drug delivery system. *J. Pharm. Sci. Res.* 12(8), 1040–1045 (2020).
25. Brück WM, Slater JW, Carney BF. Chitin and chitosan from marine organisms. in: kim s.-k, ed. chitin, chitosan, oligosaccharides and their derivatives. *Chitin, Chitosan, Oligosaccharides and Their Derivatives, Vol. 1.* Kim S (Ed.). CRC Press, FL, USA (2011).

26. Smith A, Perelman M, Hinchcliffe M. Chitosan - a promising safe and immune-enhancing adjuvant for intranasal vaccines. *Hum. Vaccin. Immunother.* 10(3), 797–807 (2014).
27. Bernkop-Schnurch A, Dunnhaupt S. Chitosan-based drug delivery systems. *Eur. J. Pharm. Biopharm.* 81(3), 463–469 (2012).
28. Naskar S, Koutsou K, Sharma S. Chitosan-based nanoparticles as drug delivery systems: a review on two decades of research. *J. Drug Target* 27(4), 379–393 (2019).
29. Li J, Cai C, Li J *et al.* Chitosan-based nanomaterials for drug delivery. *Molecules* 23(10), 2661–2684 (2018).
30. Bruinsmann FA, Vaz GR, Alves ACS *et al.* Nasal drug delivery of anticancer drugs for the treatment of glioblastoma: preclinical and clinical trials. *Molecules* 24(23), 4312–4344 (2019).
31. Samaridou E, Alonso MJ. Nose-to-brain peptide delivery – the potential of nanotechnology. *Bioorg. Med. Chem.* 26(10), 2888–2905 (2018).
32. Upadhaya PG, Pulakkat S, Patravale VB. Nose-to-brain delivery: exploring newer domains for glioblastoma multiforme management. *Drug Deliv. Transl. Res.* 10(4), 1044–1056 (2020).
33. Fessi H, Puisieux F, Devissaguet JP *et al.* Nanocapsule formation by interfacial polymer deposition following solvent displacement. *Int. J. Pharm.* 55, R1–R4 (1989).
- **First paper on the interfacial deposition of preformed polymer method.**
34. International Conference on Harmonization. ICH Topic Q2 (R1) validation of analytical procedures: text and methodology (1994). [www.ich.org/fileadmin/PublicWebSite/ICHProducts/Guidelines/Quality/Q2R1/Step4/Q2R1\\_Guideline.pdf](http://www.ich.org/fileadmin/PublicWebSite/ICHProducts/Guidelines/Quality/Q2R1/Step4/Q2R1_Guideline.pdf)
- **Paper on international guidelines for the validation of analytical procedures.**
35. Chou TC. Drug combination studies and their synergy quantification using the Chou–Talalay method. *Cancer Res.* 70(2), 440–446 (2010).
36. Chou TC. Theoretical basis, experimental design, and computerized simulation of synergism and antagonism in drug combination studies. *Pharmacol. Rev.* 58(3), 621–81 (2006).
- **Important paper for understanding the Chou–Talalay method on drug combinations and synergistic effect.**
37. Chou TC, Motzer RJ, Tong Y, Bosl GJ. Computerized quantitation of synergism and antagonism of taxol, topotecan, and cisplatin against human teratocarcinoma cell growth: a rational approach to clinical protocol design. *J. Natl. Cancer Inst.* 86(20), 1517–1524 (1994).
38. Zhang N, Fu JN, Chou TC. Synergistic combination of microtubule targeting anticancer fludelon with cytoprotective panaxytriol derived from panax ginseng against MX-1 cells in vitro: experimental design and data analysis using the combination index method. *Am. J. Cancer Res.* 6(1), 97–104 (2016).
39. Figueiró F, de Oliveira CP, Rockenbach L *et al.* Pharmacological improvement and preclinical evaluation of methotrexate-loaded lipid-core nanocapsules in a glioblastoma model. *J. Biomed. Nanotechnol.* 11(10), 1808–18 (2015).
40. Scholl JN, Dias AF, Pizzato PR *et al.* Characterization and antiproliferative activity of glioma-derived extracellular vesicles. *Nanomedicine (Lond.)* 15(10), 1001–1018 (2020).
41. Bianchin MD, Küllkamp-Guerreiro IC, Oliveira CP *et al.* Radar charts based on particle sizing as an approach to establish the fingerprints of polymeric nanoparticles in aqueous formulations. *J. Drug Deliv. Sci. Technol.* 30, 180–189 (2016).
42. Oliveira CP, Venturini CG, Donida B *et al.* An algorithm to determine the mechanism of drug distribution in lipid-core nanocapsule formulations. *Soft Matter* 9(4), 1141–50 (2013).
43. Bézivin C, Tomasi F, Lohézie-Le D, Boustie J. Cytotoxic activity of some lichen extracts on murine and human cancer cell lines. *Phytomedicine* 10(6–7), 499–503 (2003).
44. Andrade P, Dias AF, Figueiró F *et al.* 1,2,3-Triazole tethered 2-mercaptobenzimidazole derivatives: design, synthesis and molecular assessment toward C6 glioma cell line. *Future Med. Chem.* 12(8), 689–708 (2020).
45. Chothiphirat A, Nittayaboon K, Kanokwiroon K *et al.* Anticancer potential of fruit extracts from *Vatica diospyroides* symington type SS and their effect on program cell death of cervical cancer cell lines. *Sci. World J.* 2019, 1–9 (2019).
46. Quispe A, Zavala C, Rojas J *et al.* Efecto citotóxico selectivo in vitro de murcin H (acetogenina de *Annona muricata*) en cultivos celulares de cáncer de pulmón. *Rev. Peru. Med. Exp. Salud Publica* 23(4), 265–269 (2006).
47. Peña-Morán OA, Villarreal ML, Álvarez-Berber L *et al.* Cytotoxicity, post-treatment recovery, and selectivity analysis of naturally occurring podophyllotoxins from *Bursera fagaroides* var. *Fagaroides* on breast cancer cell lines. *Molecules* 21(8), 1013–1028 (2016).
48. Kreuter J, Ramge P, Petrov V *et al.* Direct evidence that polysorbate-80-coated poly(butylcyanoacrylate) nanoparticles deliver drugs to the CNS via specific mechanisms requiring prior binding of drug to the nanoparticles. *Pharm. Res.* 20(3), 409–416 (2003).
49. Sun W, Xie C, Wang H, Hu Y. Specific role of polysorbate 80 coating on the targeting of nanoparticles to the brain. *Biomaterials* 25(15), 3065–3071 (2004).
50. Kreuter J. Drug delivery to the central nervous system by polymeric nanoparticles: what do we know? *Adv. Drug Delivery Rev.* 71, 2–14 (2014).

51. Lombardo SM, Schneider M, Türeli AE, Türeli NG. Key for crossing the BBB with nanoparticles: the rational design. *Beilstein J. Nanotechnol.* 11, 866–883 (2020).
- **Paper about strategies that can be used to increase the permeation of BBB nanoparticles.**
52. Chacko BJ, Palanisamy S, Gowrishankar NL *et al.* Effect of surfactant coating on brain targeting polymeric nanoparticles. *Indian J. Pharm. Sci.* 80, 215–222 (2018).
53. Caprificov AE, Foot PJS, Polycarpou E, Calabrese G. Overcoming the blood-brain barrier: functionalised chitosan nanocarriers. *Pharmaceutics.* 12(11), 1013–1033 (2020).
54. Ojeda-Hernández DD, Canales-Aguirre AA, Matias-Guiu J *et al.* Potential of chitosan and its derivatives for biomedical applications in the central nervous system. *Front. Bioeng. Biotechnol.* 8(389), 1–15 (2020).
55. Cortés H, Alcalá-Alcalá S, Caballero-Florán IH *et al.* A reevaluation of chitosan-decorated nanoparticles to cross the blood–brain barrier. *Membranes* 10(9), 212–233 (2020).
56. Honary S, Zahir F. Effect of zeta potential on the properties of nano-drug delivery systems – a review (part 1). *Trop. J. Pharm. Res.* 12(2), 255–264 (2013).
57. Cafaggi S, Russo E, Stefani R *et al.* Preparation and evaluation of nanoparticles made of chitosan or N-trimethyl chitosan and a cisplatin–alginate complex. *J. Control. Release* 121, 110–123 (2007).
58. Nowak M, Brown TD, Graham A *et al.* Size, shape, and flexibility influence nanoparticle transport across brain endothelium under flow. *Bioeng. Transl. Med.* 5(2), 1–11 (2019).
59. Mahmoud BS, AlAmri AH, McConville C. Polymeric nanoparticles for the treatment of malignant gliomas. *Cancers (Basel).* 12(1), 175–203 (2020).
60. Müller CR, Schaffazick SR, Pohlmann AR *et al.* Spray-dried diclofenac-loaded poly(epsilon-caprolactone) nanocapsules and nanospheres. Preparation and physicochemical characterization. *Pharmazie.* 56(11), 864–867 (2011).
61. Cruz L, Schaffazick SR, Costa TD *et al.* Physico-chemical characterization and in vivo evaluation of indomethacin ethyl ester-loaded nanocapsules by PCS, TEM, SAXS, interfacial alkaline hydrolysis and antiedematogenic activity. *J. Nanosci. Nanotechnol.* 6(9–10), 3154–3162 (2006).
62. Siqueira NM, Contri RV, Paese K *et al.* Innovative sunscreen formulation based on benzophenone-3-loaded chitosan-coated polymeric nanocapsules. *Skin Pharmacol. Physiol.* 24(3), 166–174 (2011).
63. Bender EA, Cavalcante MF, Adorne MD *et al.* New strategy to surface functionalization of polymeric nanoparticles: one-pot synthesis of scFv anti-LDL(–)-functionalized nanocapsules. *Pharm. Res.* 31, 2975–2987 (2014).
64. Cé R, Marchi JG, Bergamo VZ *et al.* Chitosan-coated dapsone-loaded lipid-core nanocapsules: growth inhibition of clinical isolates, multidrug-resistant *Staphylococcus aureus* and *Aspergillus* ssp. *Colloids Surf. A Physicochem. Enginer. Aspects* 511, 153–161 (2016).
65. Jiang P, Mukthavaram R, Chao Y *et al.* Novel anti-glioblastoma agents and therapeutic combinations identified from a collection of FDA approved drugs. *J. Transl. Med.* 12, 1–13 (2014).
66. Ghosh D, Nandi S, Bhattacharjee S. Combination therapy to checkmate glioblastoma: clinical challenges and advances. *Clin. Transl. Med.* 7(1), 33–45 (2018).
67. Erdő F, Bors LA, Farkas D *et al.* Evaluation of intranasal delivery route of drug administration for brain targeting. *Brain Res. Bull.* 143m, 155–170 (2018).
68. Pires PC, Santos AO. Nanosystems in nose-to-brain drug delivery: a review of non-clinical brain targeting studies. *J. Control Release.* 270, 89–100 (2018).
69. Bourganis V, Kammona O, Alexopoulos A, Kiparissides C. Recent advances in carrier mediated nose-to-brain delivery of pharmaceuticals. *Eur. J. Pharm. Biopharm.* 128, 337–362 (2018).
70. Djupesland PG, Messina JC, Mahmoud RA. The nasal approach to delivering treatment for brain diseases: an anatomic, physiologic, and delivery technology overview. *Ther. Deliv.* 5(6), 709–733 (2014).
71. Krishnan JKS, Arun P, Chembukave B *et al.* Effect of administration method, animal weight and age on the intranasal delivery of drugs to the brain. *J. Neurosci Methods.* 286, 16–21 (2017).
72. Gao M, Shen X, Mao S. Factors influencing drug deposition in the nasal cavity upon delivery via nasal sprays. *J. Pharm. Investig.* 50, 251–259 (2020).
73. Gänger S, Schindowski K. Tailoring formulations for intranasal nose-to-brain delivery: a review on architecture, physico-chemical characteristics and mucociliary clearance of the nasal olfactory mucosa. *Pharmaceutics.* 10(3), 116–144 (2018).
74. Azambuja JH, Schuh RS, Michels LR *et al.* Nasal administration of cationic nanoemulsions as CD73-siRNA delivery system for glioblastoma treatment: a new therapeutical approach. *Mol. Neurobiol.* 57(2), 635–649 (2020).
75. Colombo M, Figueiró F, Dias AF *et al.* Kaempferol-loaded mucoadhesive nanoemulsion for intranasal administration reduces glioma growth in vitro. *Int. J. Pharm.* 543(1–2), 214–223 (2018).
76. Bahmanpour AH, Ghaffari M, Ashraf S, Mozafari M. Nanotechnology for pulmonary and nasal drug delivery. *Nanoengineer. Biomat. Adv. Drug Delivery* 561–579 (2020).

77. Ortiz M, de Sa Coutinho D, Ciambarella BT *et al.* Intranasal administration of budesonide-loaded nanocapsule microagglomerates as an innovative strategy for asthma treatment. *Drug Deliv. Transl. Res.* 10(6), 1700–1715 (2020).
78. Kang C, Yuan X, Zhong Y *et al.* Growth inhibition against intracranial C6 glioma cells by stereotactic delivery of BCNU by controlled release from poly(D,L-lactic acid) nanoparticles. *Technol. Cancer Res. Treat.* 8(1), 61–70 (2009).
79. Shi J, Zhang Y, Fu W *et al.* Establishment of C6 brain glioma models through stereotactic technique for laser interstitial thermotherapy research. *Surg Neurol Int.* 6, 51–58 (2015).
80. Azambuja JH, Schuh RS, Michels LR *et al.* CD73 as a target to improve temozolomide chemotherapy effect in glioblastoma preclinical model. *Cancer Chemother. Pharmacol.* 85(6), 1177–1182 (2020).